Materials Science & Engineering A 832 (2022) 142422

Contents lists available at ScienceDirect

Materials Science & Engineering A

journal homepage: www.elsevier.com/locate/msea

Synergistic effects of Cd, Si and Cr additions on precipitation strengthening and thermal stability of dispersoids in AA3003 alloy

Feng Qian [a,b,c], Shenbao Jin [d], Di Wan [e], Wenzhe Li [a], Xingwang Cheng [a,b], Gang Sha [d], Yanjun Li [c,*]

[a] School of Materials Science and Engineering, Beijing Institute of Technology, 100081, Beijing, China
[b] China National Key Laboratory of Science and Technology on Materials Under Shock and Impact, Beijing Institute of Technology, Beijing, 10081, China
[c] Department of Materials Science and Engineering, Norwegian University of Science and Technology, 7491, Trondheim, Norway
[d] School of Materials Science and Engineering, Herbert Gleiter Institute of Nanoscience, Nanjing University of Science and Technology, 210094, Nanjing, China
[e] Department of Mechanical and Industrial Engineering, Norwegian University of Science and Technology, Trondheim, 7491, Norway

ARTICLE INFO

Keywords:
α-Al(Mn,Fe)Si dispersoids
Precipitation strengthening
Microalloying
Aluminium alloys
High-temperature applications
Atom probe tomography (APT)

ABSTRACT

The thermally stable Mn-rich dispersoids in Al alloys were recently reported to have a significant dispersion strengthening effect. Further improvements in the dispersion strengthening and thermal stability of Mn-rich dispersoids are required to achieve satisfactory mechanical properties for elevated temperature applications. This study reports that, with minor additions of Cd, Cr and increased Si content, the yield strength of the modified AA3003 alloy is increased by 39% compared to the base alloy subjected to the same heat treatment. Moreover, the thermal stability of the modified alloy when exposed to a long-term thermal holding up to 1000 h at 400 °C is greatly improved. Microstructural characterizations reveal that the dispersoids in the modified alloy are greatly refined, and their distribution is more homogeneous compared to the base alloy. It is observed that the Cd-rich clusters/nanoparticles formed in the initial stage of heat treatment, can effectively "attract" dispersoid-forming atoms (e.g. Mn, Si and Cr) and subsequently lead to a heterogeneous nucleation of dispersoids on them, which is responsible for the enhanced dispersoid precipitation and dispersion strengthening in the modified alloy. The partitioning of the low-diffusivity peritectic element Cr into dispersoids can improve the thermal stability and increase the number density of dispersoids in the centre of dendrite arms, which also contributes to the promising mechanical properties of the modified alloy.

1. Introduction

Aluminium (Al) alloys, which possess high specific strength, as well as excellent corrosion resistance, weldability and formability, are the most important light-weight metallic materials in the automotive and aerospace industries. However, for the most extensively used high-strength Al alloys, i.e. precipitation-strengthened 2/6/7xxx Al alloys, the thermal stability of strengthening precipitates is generally poor, which significantly limits their usage in weight-sensitive, high-temperature applications (≥250 °C). Researchers are dedicated to developing new Al alloys strengthened by second-phase particles with good thermally stability. The Al–Sc system and its derivatives, which can produce a high density of $L1_2$-structured Al_3Sc precipitates with good thermal stability via aging, are considered as promising precipitation-strengthened Al alloys for certain high-temperature applications [1–3]. However, Sc is extremely expensive. Efforts have been made to find less costly substituting elements for Sc, but currently even a partial substitution of Sc causes a significant sacrifice of precipitation strengthening [4].

Mn-rich dispersoids, which are generally formed in 3/5/6xxx alloys during high-temperature heat treatments, have also been reported to be thermal stable. However, due to the difficulty in nucleation, the number density of Mn-rich dispersoids in these alloys is normally very low [5–7]. As a result, their contribution to dispersion strengthening has been considered negligible [8–10]. Recently, it is found that significant dispersion strengthening by α-Al(Mn,Fe)Si dispersoids at room and elevated temperatures can be achieved in 3xxx alloys via appropriate heat treatments [10–13] or modification of alloy compositions [14–16]. It was reported that an increase in yield strength (YS) by 54% could be achieved in 3003 alloy [10]. A compression YS as high as 78 MPa tested

* Corresponding author.
E-mail address: yanjun.li@ntnu.no (Y. Li).

https://doi.org/10.1016/j.msea.2021.142422
Received 9 September 2021; Received in revised form 23 November 2021; Accepted 26 November 2021
Available online 27 November 2021

at 300 °C was reported in a dispersion-strengthened 3004 alloy, and the YS stayed at 77 MPa even after holding for 1000 h [11]. Microalloying additions were proved to further improve the strengthening contributions of dispersoids in 3xxx alloys [17–19]. The present authors reported a superior precipitation strengthening response with a minor Cd addition which led to increase of YS by 25% in a 3003 alloy [20] and by 57% in a 6082 alloy [26].

To further improve the thermal stability of α-Al(Mn,Fe)Si dispersoids, additions of alloying elements with lower diffusivities in Al, such as Mo [19,21] have been attempted. The partitioning of Mo into α-Al (Mn,Fe)Si dispersoids could significantly improve the thermal stability of the dispersoids in Al alloys [19,21]. As a dispersoid-forming element [6,22,23], Cr also has a much lower diffusivity than Mn in Al (e.g. $7.2\times 10^{-14}\ cm^2s^{-1}$ vs. $1.1\times 10^{-9}\ cm^2s^{-1}$ at 450 °C, respectively) [24,25]. Therefore, it is expected that Cr can reduce the coarsening rate of dispersoids.

By combining the two aims of (i) increasing the number density of α-Al(Mn,Fe)Si dispersoids and (ii) further improving the thermal stability of dispersoids, this work focuses on a new 3003 alloy microalloyed with Cd, Si and Cr. It is shown that a significantly enhanced dispersion strengthening and good thermal stability at high temperatures have been achieved in the alloy. The influences of alloying additions on the number density, distribution, size and chemical composition of dispersoids in AA3003 alloys during heat treatment were examined. Moreover, the roles of alloying elements in promoting the nucleation and precipitation kinetics of the dispersoids were studied.

2. Experimental

Two experimental 3003Si and 3003SiCdCr alloys were prepared. A commercial DC-cast 3003 alloy was first melted in a crucible in induction furnace, and solar-grade pure Si, Al-5 wt% Cd and Al-10 wt% Cr master alloys were then added at 750–780 °C. After a complete dissolution of all the adding elements, the melt was cast into a copper mould with dimensions of $100\times 70\times 30\ mm^3$. The cooling rate of the ingot is about ~50 K/s. At this cooling rate, most of Cd could be kept in the solid solution, and few Cd-rich constituent particles could be detected in the solidification structure. The chemical compositions of the experimental alloys were determined by inductively coupled plasma optical emission spectroscopy (ICP-OES) and presented in Table 1, along with that of the 3003Cd and 3003 base alloys for comparison. The preparation of the latter two alloys was described in Ref. [20].

Samples cut from each as-cast ingot were continuously heated to 600 °C at a rate of 50 °C/h. To monitor the precipitation behaviour of dispersoids during heat treatment, 10 samples were water quenched one by one at a temperature interval of 50 °C during the heating process between 150 and 600 °C. To evaluate the thermal stability of dispersoids, a long-term thermal holding at 400 °C up to 1000 h was carried out on the four alloys as-heated to peak hardness by continuous heating. Vickers hardness of as-cast and heat-treated samples was measured with a Matsuzawa hardness tester under a 5 kg load and a dwell time of 15 s. Each hardness result was an average of at least eight measurements. The electrical conductivity (EC) measurements were conducted at room temperature (RT) using Foerster Sigmatest 2.069 instrument. Flat rectangular tensile samples were machined based on ASTM standard with a gage length of 25 mm. Room-temperature tensile testing was carried out on an MTS 810 tensile testing machine at an initial strain rate of 0.001 s^{-1}, and at least two samples were tested for each condition.

Transmission electron microscopy (TEM) disks were first thinned to a thickness of ~100 μm by a standard mechanical polishing procedure, and further twin-jet electropolished using a solution of 1/3 HNO_3 in methanol at −25 °C with a voltage of ~20 V. Overview observations of the dispersoid distribution were performed on the TEM disks by using a Thermo Fisher Quanta 650 FEG-SEM equipped with a solid-state four-quadrant backscattered electron (BSE) detector. A JEOL 2100 TEM operated at 200 kV was employed to obtain bright-field TEM images for quantitative analyses of dispersoids. The number density of dispersoids is determined as $N_V=\frac{N}{A(\overline{D}+t)}$ [7], where N is the counted number of dispersoids within the TEM image, A is the area of the image, $\overline{D}$ is the average equivalent diameter of dispersoids and t is the foil thickness of the imaging area measured by electron energy loss spectroscopy (EELS). At least six TEM images from the centre to the periphery of dendrite arms were taken and analysed for each sample. For the compositional analyses of dispersoids, a JEOL 2100F TEM operated at 200 kV was employed to acquire HAADF-STEM images and the corresponding energy dispersive X-ray spectroscopy (EDS) data.

The elemental distributions of dispersoid in the early stage precipitation were characterized by APT. The needle-shaped APT samples were prepared by etching square rod samples ($0.5\times 0.5\times 15\ mm^3$) with a standard two-step electropolishing procedure: (1) a solution of 30% perchloric acid in acetic acid at 20 V and (2) a solution of 5% perchloric acid in 2-butoxyethanol at 20 V. The APT characterization was performed on a LEAP4000X SI local electrode atom probe at a sample temperature of 20 K, under a high vacuum of 2×10^{-9} Pa. The UV laser pulsing mode was used with a laser pulse energy of 40 pJ, a repetition rate of 250 kHz and a target evaporation rate of 0.5% (5 ions per 1000 pulses). Cameca IVAS 3.6.12 was used for the data reconstruction and statistical analyses.

Table 1
Chemical compositions of the experimental alloys (wt %).

Alloy	Mn	Fe	Si	Cd	Cr	Al
3003SiCdCr	1.08	0.58	0.50	0.20	0.15	bal.
3003Si	1.00	0.50	0.49	–	–	bal.
3003Cd [20]	1.10	0.50	0.18	0.21	–	bal.
3003 [20]	1.11	0.56	0.16	–	–	bal.

3. Results and discussion

3.1. Mechanical properties and electrical conductivity

3.1.1. Evolution of hardness and electrical conductivity

The evolution of Vickers hardness and electrical conductivity (EC) of the 3003SiCdCr alloys during heating from RT to 600 °C at 50 °C/h is shown in Fig. 1. The data of the 3003, 3003Si and 3003Cd alloys is also included for comparison [20]. As shown in Fig. 1(a), in the as-cast state, 3003Si and 3003SiCdCr alloys exhibit slightly higher hardness and lower EC than the 3003 and 3003Cd alloys, due to the increased solid solution of Si in the former two alloys. Within the temperature range between 150 and 600 °C, the hardness of the 3003SiCdCr alloy is much higher than that of the other three alloys. Especially at the peak hardness achieved at 450 °C, the hardness of the 3003SiCdCr alloy is 53.6 ± 0.8 HV, while that of the 3003, 3003Si and 3003Cd alloy is 44.3 ± 0.6, 47.2 ± 0.7 and 49.2 ± 0.5 HV, respectively. Additionally, the maximum increase of EC (7.4 MS/m) corresponding to the decomposition of solid solution and dispersoid precipitation in the 3003SiCdCr alloy is much greater than that of the other three alloys (see Fig. 1(b)). It is also worth noting that during heating from 450 to 500 °C, the hardness decrease of the 3003SiCdCr alloy is much smaller than that of the 3003Si and 3003Cd alloys: the hardness decreases by 1.2% in the 3003SiCdCr alloy, compared to 3.1% and 7.3% in the 3003Si and 3003Cd alloys, respectively. Besides, the EC of the 3003SiCdCr alloy keeps increasing up to 500 °C, indicating an ongoing decomposition of supersaturated solid solution in the 3003SiCdCr alloy until heating to 500 °C.

In addition, a distinct hardness peak at 200 °C is observed in both the 3003Cd and the 3003SiCdCr alloys (Fig. 1(a)), which indicates the precipitation of Cd-rich nanoparticles [20]. Different from the 3003Cd alloy, the hardness increase has already started as early as 150 °C in the 3003SiCdCr alloy. Correspondingly, the EC of 3003SiCdCr alloy also increases steadily from as early as 150 °C, in contrast to the nearly

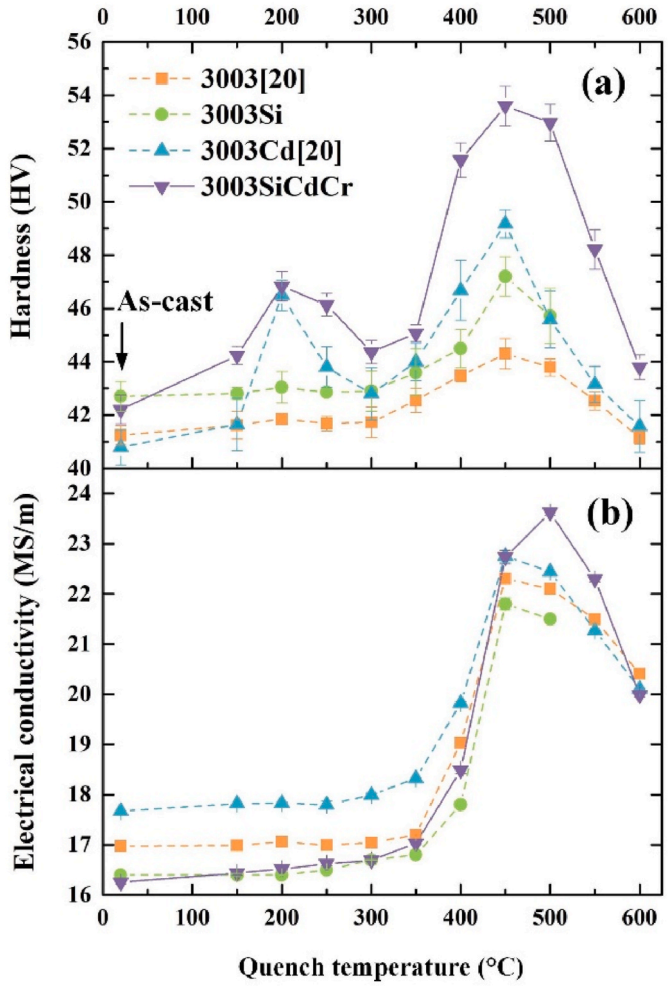

Fig. 1. Evolution of (a) Vickers hardness and (b) electrical conductivity of 3003 [20], 3003Si, 3003Cd [20], 3003SiCdCr alloys during heating from RT to 600 °C at a heating rate of 50 °C/h. The samples are water quenched into cold water one by one at a temperature interval of 50 °C. The hardness of the 3003SiCdCr alloy is much higher than that of the other three alloys at all heating temperatures.

constant EC values of the other three alloys below 300 °C. In addition, the hardness decrease after the first peak hardness is slower in the 3003SiCdCr alloy than that of the 3003Cd alloy, implying that the coarsening kinetics of Cd-rich nanoparticles is also slower.

3.1.2. Tensile properties

Room-temperature tensile tests have been conducted on the four alloys as-heated to either 450 °C or 500 °C with a rate of 50 °C/h and the representative engineering stress-strain curves are shown in Fig. 2. The corresponding mechanical properties, such as YS, ultimate tensile strength (UTS) and total elongation (TE) are listed in Table 2. For the samples as-heated to peak hardness at 450 °C, the YS of the 3003SiCdCr alloy is 96 ± 1 MPa, which is 39%, 19% and 12% higher than that of the 3003, 3003Si and 3003Cd alloys, respectively. For the samples as-heated to 500 °C, the YS of the 3003SiCdCr alloy is 94 ± 1 MPa, which remains almost at the same level as that of the alloy as-heated to 450 °C (Table 2). In contrast, the YS of the 3003Cd alloy is reduced to 79 ± 1 MPa, which is 8% lower than that of the sample as-heat to 450 °C.

3.1.3. Thermal stability

To evaluate the thermal stability of dispersoids at elevated temperatures, a long-term annealing at 400 °C up to 1000 h was carried out on the four alloys as-heated to 450 °C with a rate of 50 °C/h (peak-hardness

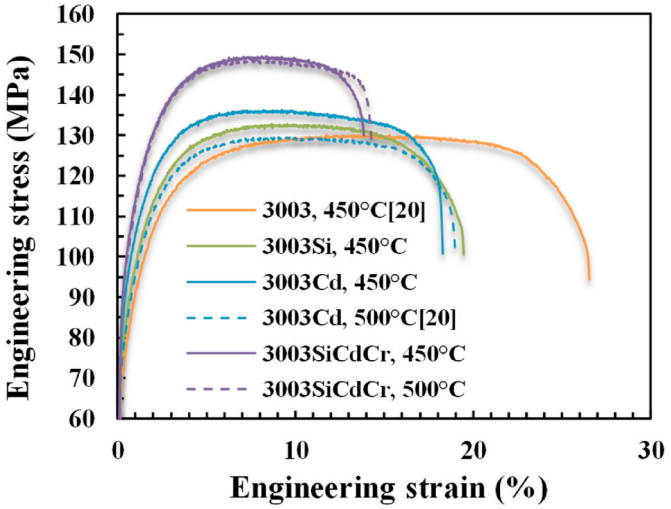

Fig. 2. Engineering stress-strain curves of the four alloys (3003 [20], 3003Si, 3003Cd [20] and 3003SiCdCr) as-heated to 450 and 500 °C with a rate of 50 °C/h, respectively. The temperature of 450 °C is where the peak hardness was achieved for the four alloys and the temperature 500 °C is selected to evaluate the alloy stability at higher temperatures. All the tensile results are based on the same dimensions of tensile samples.

Table 2
Mechanical properties of the 3003, 3003Si, 3003Cd and 3003SiCdCr alloys subjected to different heat treatments.

Samples	YS (MPa)	UTS (MPa)	TE (%)
3003, 600 °C_24h [20]	49 ± 1	126 ± 1	25.8 ± 0.4
3003, 450 °C [20]	69 ± 2	128 ± 2	25.9 ± 2.1
3003Si, 450 °C	81 ± 2	132 ± 1	15.9 ± 1.9
3003Cd, 450 °C [20]	86 ± 2	136 ± 2	17.7 ± 0.6
3003Cd, 500 °C	79 ± 1	129 ± 1	20.5 ± 1.8
3003SiCdCr, 450 °C	96 ± 1	149 ± 1	14.9 ± 2.2
3003SiCdCr, 500 °C	94 ± 1	148 ± 1	13.6 ± 2.1

treatment). The corresponding Vickers hardness vs. annealing time curves are plotted in Fig. 3. The 3003 and 3003Si alloys experienced a sharp decrease of hardness with time, and the hardness is decreased by

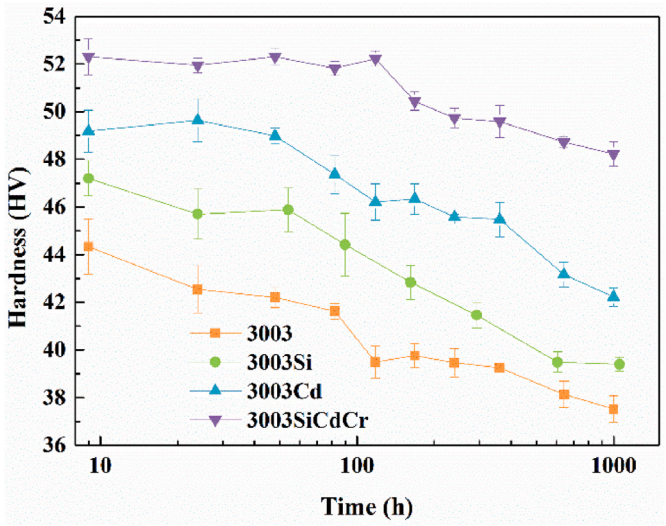

Fig. 3. Evolution of Vickers hardness of the 3003, 3003Si, 3003Cd and 3003SiCdCr alloys when annealing at 400 °C. The four tested samples were continuously heated to 450 °C (peak-hardness treatment) and water quenched before annealing at 400 °C.

15.3% and 16.5%, respectively, after 1000 h annealing. The hardness of the 3003Cd alloy is slightly increased in the first 24 h probably due to the further precipitation of dispersoids. With further increasing annealing time up to 1000 h, however, the hardness gradually reduces to 42.2 HV, which is 14.2% lower than the hardness before annealing. For the 3003SiCdCr alloy, no evident decrease of hardness is observed until annealing for 168 h, and the total decrease of hardness after 1000 h is only 7.8% which is much smaller than that of the other three alloys.

3.2. Microstructural characterization

3.2.1. Precipitation of dispersoids

Fig. 4 presents the TEM images of the 3003SiCdCr alloy during heating between 250 and 550 °C. As can be seen in Fig. 4(a), a large number of ultrafine nanoparticles enriched with Cd (see inset) have formed in the 3003SiCdCr alloy as-heated to 250 °C, which confirms that the first peak hardness in Fig. 1 is associated with Cd-rich nanoparticles. According to the quantitative analyses, the number density of Cd-rich nanoparticles in the 3003SiCdCr alloy as-heated to 250 °C is 2.4×10^4 μm^{-3} which is almost twice that of the 3003Cd alloy (1.3×10^4 μm^{-3} [20]), and this is responsible for the higher hardness of the 3003SiCdCr alloy than that of the 3003Cd alloy at 250 °C. After continuous heating to 350 °C, two types of particles can be observed: larger Cd-rich nanoparticles with dark contrast and smaller, denser α-Al(Mn,Fe)Si dispersoids with grey contrast [20] (Fig. 4(b)). A closer observation shows that some of the α-Al(Mn,Fe)Si dispersoids are attached to Cd-rich nanoparticles (see inset). Further increasing temperature up to 400 and 450 °C leads to the growth of α-Al(Mn,Fe)Si dispersoids accompanied by the dissolution of Cd-rich nanoparticles (Fig. 4 (c) and (d)). After heating to 500 °C, a slight increase in the size of the dispersoids can be observed, while the number density is decreased (Fig. 4(e)). In the sample as heated to 550 °C, an obvious increase in size and a significant reduction in number density can be observed (Fig. 4 (f)).

The equivalent diameter and number density of α-Al(Mn,Fe)Si dispersoids in the 3003SiCdCr alloy at different heating temperatures, together with the statistical data of the 3003 and 3003Cd alloys [20], are plotted in Fig. 5. In the temperature range 400–550 °C, the equivalent diameter of dispersoids in the 3003SiCdCr alloy is significantly smaller than that in the 3003 and 3003Cd alloys at the same temperatures, and this is more evident at 500 and 550 °C (Fig. 5(a)). Correspondingly, the number density of dispersoids in the 3003SiCdCr alloy is much higher than that of the other two alloys at the same temperatures between 350 and 500 °C (Fig. 5(b)), especially at 500 °C, indicating that the dispersoids in the 3003SiCdCr alloy have a much higher thermal stability at elevated temperatures. This is supposed to be responsible for the higher hardness of the 3003SiCdCr alloy at 450–500 °C than the other alloys, as presented in Fig. 1(b).

Fig. 6 shows the HAADF-STEM image and corresponding EDS maps of the 3003SiCdCr alloy as-heated to 450 °C. It can be seen that the particles with grey contrast comprise Mn, Fe and Si, confirming that they are α-Al(Mn,Fe)Si dispersoids. A higher level of Cr in some of the dispersoids than in the Al matrix can also be observed (indicated by white arrows in the Cr map), which implies that Cr has partitioned into dispersoids at 450 °C. Besides, the elemental maps also demonstrate that the small precipitates adjacent to the dispersoids are enriched with Cd, as indicated by white arrows in the Cd map (Fig. 6(f)).

3.2.2. Distribution of dispersoids

To get an overview about the dispersoid distribution in grains and dendrite arms, SEM images were taken on the four alloys as-heated to 450 °C, see Fig. 7. In the 3003 alloy, the number density of dispersoids in the Al matrix is rather low and some local regions in the centre of dendrite arms are free of dispersoids (Fig. 7(a)) due to the depletion of

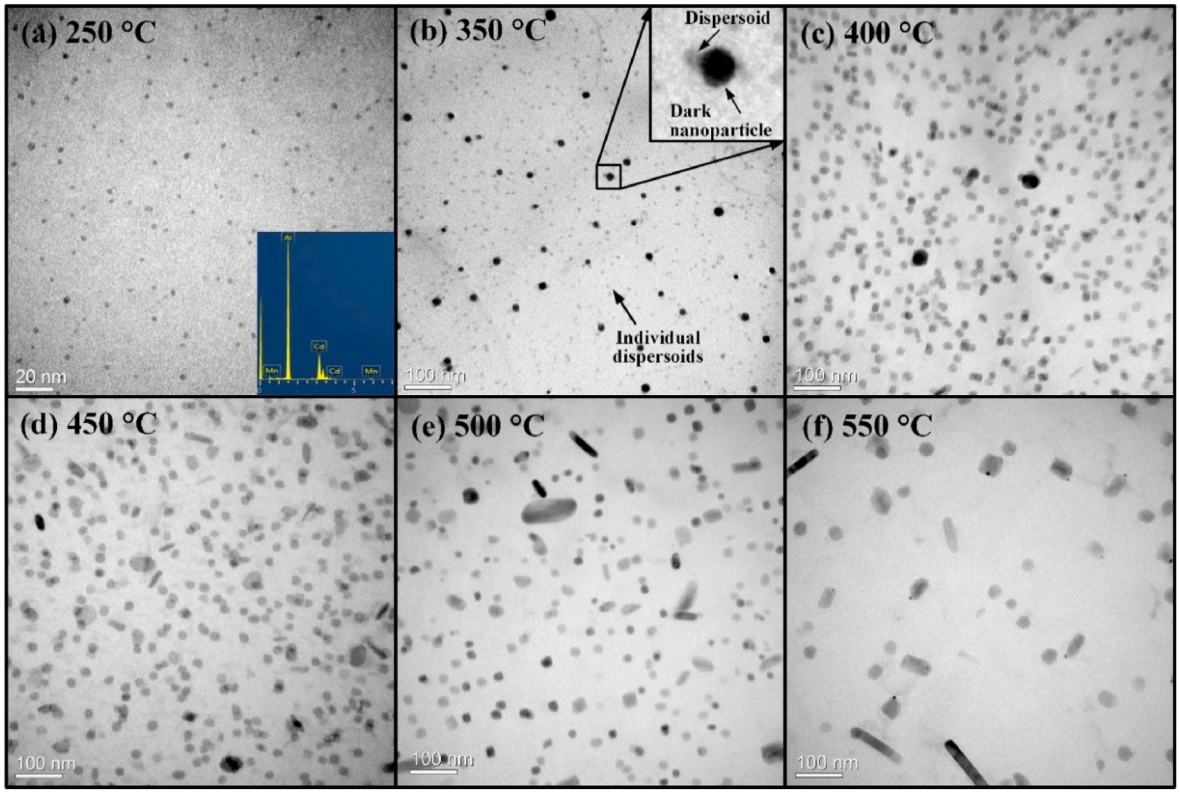

Fig. 4. TEM micrographs of the 3003SiCdCr alloy as-heated to (a) 250 °C; (b) 350 °C; (c) 400 °C; (d) 450 °C; (e) 500 °C and (f) 550 °C. The dense nanoparticles formed at 250 °C are Cd-rich nanoparticles. At 350 °C, both larger Cd-rich nanoparticles with dark contrast and smaller, denser α-Al(Mn,Fe)Si dispersoids with grey contrast can be observed. In the temperature range 400–550 °C, the dispersoids were gradually growing and coarsening.

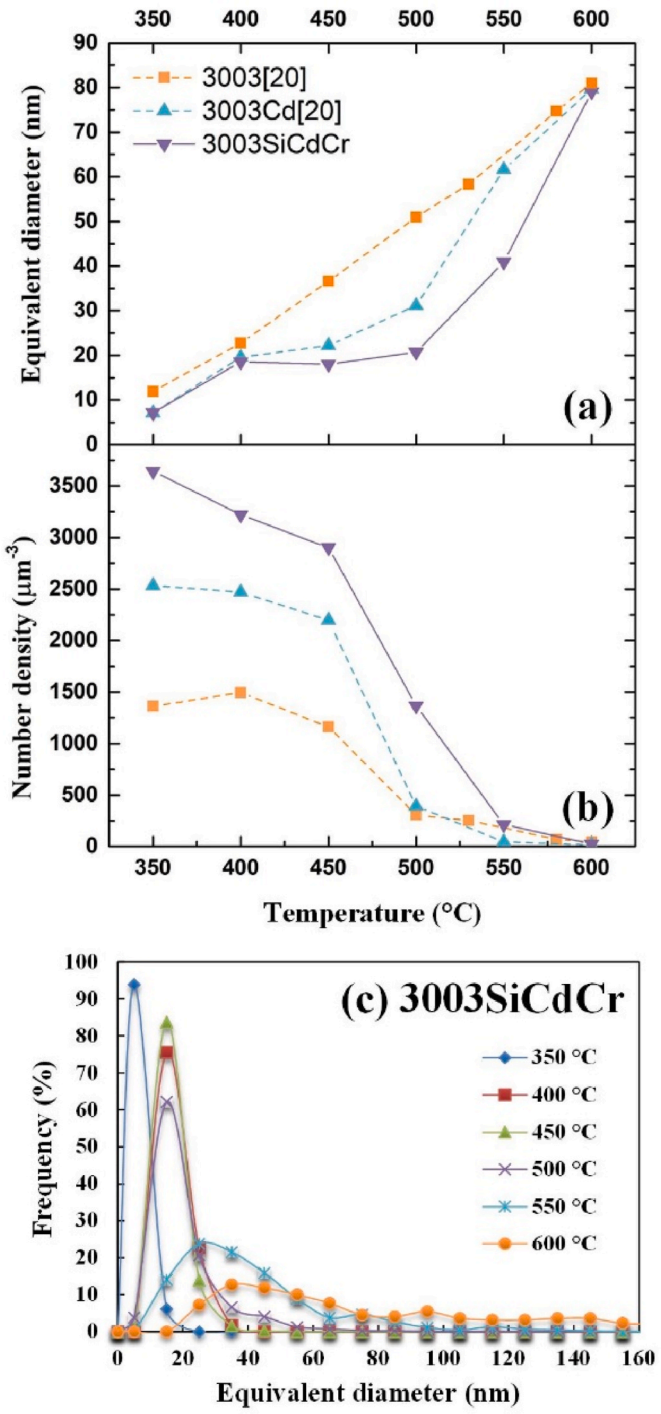

Fig. 5. (a) Equivalent diameter and (b) number density of dispersoids in the 3003 [20], 3003Cd [20] and 3003SiCdCr alloys as-heated to 350–600 °C; (c) size distribution of dispersoids at different temperatures in the 3003SiCdCr alloy. The deviation of equivalent diameter is given in the form of size distribution.

eutectic element Mn at the centre of dendrite arms [27]. Increasing Si content leads to more dispersoids in the 3003Si alloy, but the precipitate-free zones (PFZ) in the dendrite centre still exist (Fig. 7(b)). In the 3003Cd alloy, dispersoids with a significantly higher number density are observed, and the fraction of PFZ in the centre of dendrite arms is reduced (Fig. 7(c)). In the 3003SiCdCr alloy, a further increased number density of dispersoids is formed in the Al matrix. Most importantly, there is no distinct PFZ in the centre of dendrites throughout the sample. Only the regions very close to dendrite arm periphery and surrounding the constituent particles are depleted in dispersoids, as shown in Fig. 7(d). It suggests that the addition of peritectic-forming element Cr has promoted the dispersoid precipitation in the centre regions of Al dendrite arms.

3.2.3. *Nucleation of dispersoids*

The Cd-rich nanoparticles formed during the initial stage of heat treatment (≤300 °C) in the 3003SiCdCr alloy were investigated by APT. Two heat treatment conditions of interest, namely as-heated to 200 and 300 °C, were selected and the corresponding APT results are shown in Fig. 8 and Fig. 9, respectively. In the APT mass spectra, peaks of alloying elements Cd, Mn, Si and Cr can be clearly identified. However, it is difficult to identify the Fe peak, as the peaks of Fe^{2+} ions are too weak to be resolved from the tail of strong Al^{+} peak in the mass spectra [28]. For the 3003SiCdCr alloy as-heated to 200 °C, as shown in Fig. 8(a), Cd-rich atomic clusters/nanoparticles with a high number density have formed in the alloy. Interestingly, Mn-rich atomic clusters can also be observed in the Mn atom map (indicated by black circles) and the locations of these Mn-rich clusters are coincident with Cd-rich clusters/nanoparticles (indicated by black circles in Cd map). In order to further resolve the elemental distribution in the Cd-rich clusters/nanoparticles, the isoconcentration surfaces (green) at 1.5 at.% Cd is utilized to define the Cd-rich clusters/nanoparticles, as shown in Fig. 8 (b). The Cd-rich clusters/nanoparticles have an average diameter of 3.58 nm and a number density of 8.2×10^4 μm^{-3}. The proximity histograms (proxigrams) of Cd, Mn, Si and Cr concentrations as a function of the distance from the isosurfaces of Cd-rich clusters/nanoparticles have been constructed, and the proxigrams of two types of Cd-rich clusters/nanoparticles are presented in Fig. 8(c) and (d). For smaller Cd-rich clusters/nanoparticles with diameters less than 4 nm (Fig. 8(c)), the Mn concentration in Cd-rich clusters/nanoparticles is significantly higher than that in the Al matrix, while the concentrations of Si and Cr around the isosurface are slightly higher than that in the matrix. For Cd-rich clusters/nanoparticles larger than 4 nm in diameter (Fig. 8(d)), in addition to the major constituent element Cd, significant enrichment of other solute atoms, such as Mn, Si and Cr, can be observed. The Mn concentration in the centre of larger Cd-rich clusters/nanoparticles is 0.63 ± 0.05 at.% compared to 0.44 ± 0.07 at.% in the smaller Cd-rich clusters/nanoparticles and 0.014 ± 0.002 at.% in the Al matrix. In addition, the concentrations of Si and Cr in the centre of Cd-rich clusters/nanoparticles are about 1.65 and 2.62 times as high as that in the Al matrix, respectively.

With increasing temperature to 300 °C, the Cd-rich nanoparticles become much larger than those formed at 200 °C, with an average diameter of 8.5 nm and a lower number density of 3.1×10^3 μm^{-3} (Fig. 9). The Cd concentration in Cd-rich nanoparticles increases to 17.1 ± 0.4 at.%, and the concentrations of other elements are also much higher: the Mn, Si and Cr concentrations in the centre of Cd-rich nanoparticles have increased to 1.39 ± 0.12, 0.84 ± 0.09 and 0.22 ± 0.05 at.%, respectively.

Based on the microstructural observations in the 3003SiCdCr alloy during continuous heating, the precipitation sequence of α-Al(Mn,Fe)Si dispersoids can be proposed as follows. During heat treatment at 150–300 °C, due to the extremely low solubility and relatively high diffusivity of Cd in Al, a large number of ultrafine Cd-rich atomic clusters/nanoparticles form in the matrix (Fig. 4(a)). Subsequently, the supersaturated solute elements in the Al solid solution, namely Mn, Si, Fe and Cr, gradually partition into Cd-rich clusters/nanoparticles (Fig. 8). Such high concentrations of dispersoid-forming elements at the local region of Cd-rich nanoparticles will greatly favour the nucleation of α-Al (Mn,Fe)Si dispersoids by reducing the nucleation energy barrier. At the same time, Cd-rich nanoparticles may also act as heterogeneous nucleation sites for dispersoids (Fig. 9), which can further reduce the nucleation energy barrier. Since the number density of Cd-rich nanoparticles at low temperatures (200–300 °C) is about 1–2 orders of magnitude

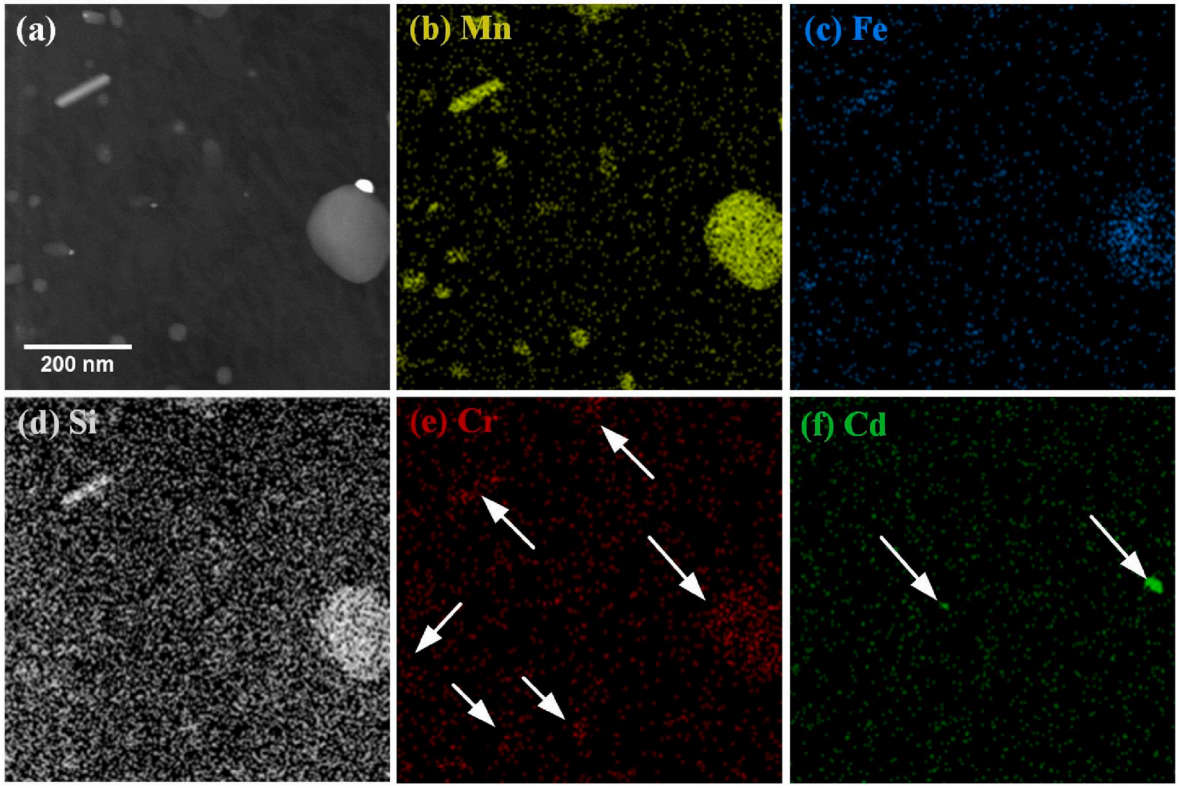

Fig. 6. (a) HAADF-STEM images of dispersoids and corresponding EDS maps of (b) Mn, (c) Fe, (d) Si, (e) Cr and (f) Cd in the 3003SiCdCr alloy as-heated to 450 °C. The enrichment of Mn, Fe, Si and a small amount of Cr in dispersoids is evident. Cd-rich nanoparticles adjacent to dispersoids are also noticed.

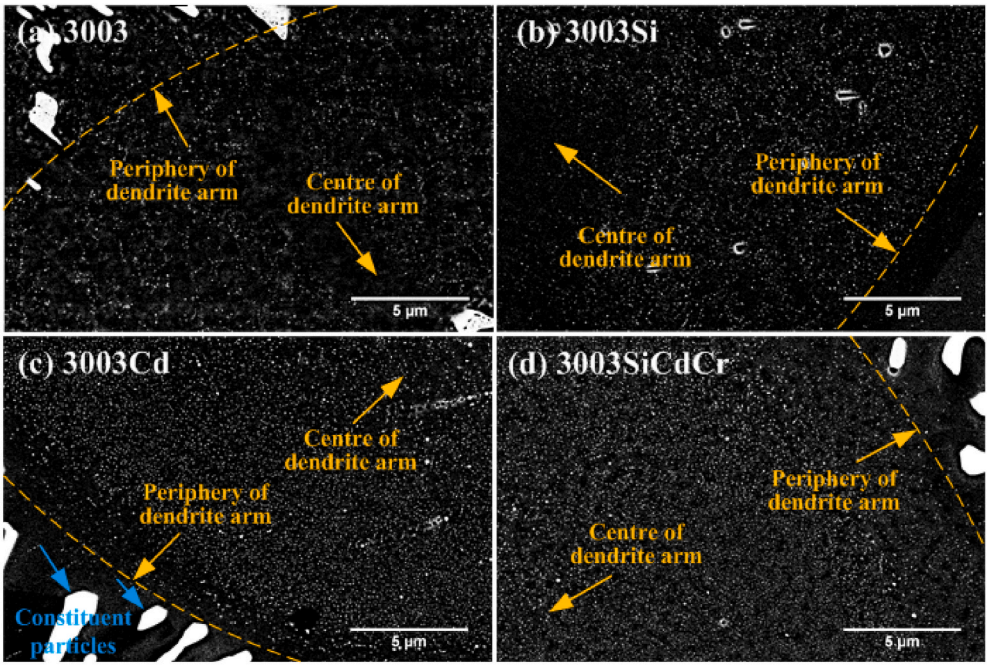

Fig. 7. SEM micrographs showing the distribution of dispersoids in the (a) 3003, (b) 3003Si, (c) 3003Cd and (c) 3003SiCdCr alloys as-heated to 450 °C. Constituent particles (blue arrows) are generally formed at the interdendritic regions. Large areas free of dispersoids are observed in the (a) 3003 and (b) 3003Si alloys, but is barely seen in the (c) 3003Cd and (d) 3003SiCdCr alloys. (For interpretation of the references to colour in this figure legend, the reader is referred to the Web version of this article.)

higher than the maximum number density of α-Al(Mn,Fe)Si dispersoids forming in AA3003 base alloy [7], it is suggested that the addition of Cd in the 3003SiCdCr alloy can provide sufficient potential nucleation sites for dispersoids. This is evidenced by the similar number density of dispersoids in the 3003SiCdCr alloy at 350 °C and the number density of Cd-rich nanoparticles precipitated at 300 °C. It is worth noting that not all the dispersoids at 350 °C are observed to be attaching to a pre-existing Cd-rich nanoparticle. This is attributed to the dissolution of some small Cd-rich nanoparticles due to coarsening during heating to higher temperatures (Fig. 4(b)). It is speculated that, however, the local enrichment of Mn, Fe, Si and Cr atoms will remain in the matrix, because most of these elements have much lower diffusivities than Cd. These atomic clusters will facilitate the nucleation of dispersoids.

In the 3003SiCdCr alloy, the higher Si content can also facilitate the

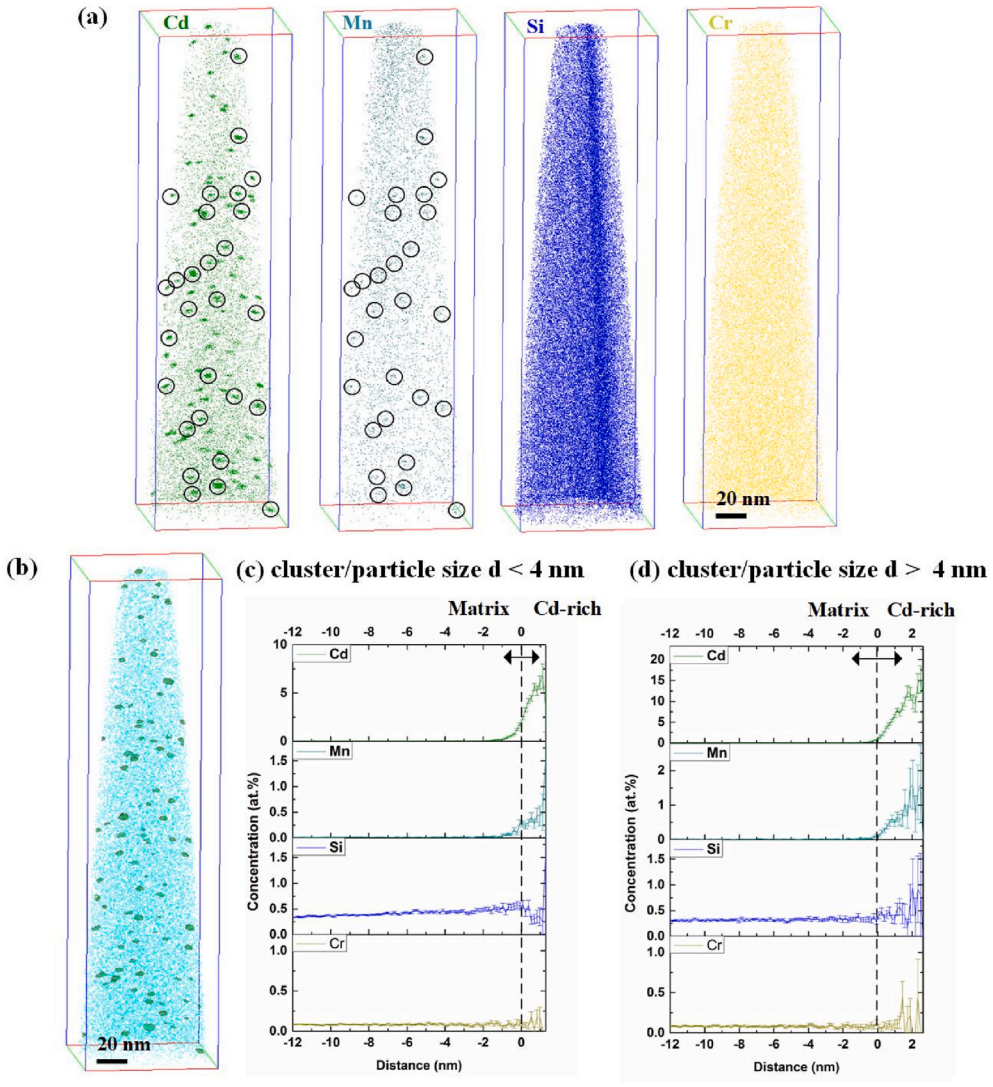

Fig. 8. Atom probe analysis of Cd-rich clusters/nanoparticles in the 3003SiCdCr alloy as-heated to 200 °C. (a) Cd (green), Mn (dark cyan), Si (blue) and Cr (yellow) atom maps; (b) tomography of Cd-rich clusters/nanoparticles identified by the 1.5 at.% Cd isosurfaces (green); proximity histogram showing the compositional change in and around the selected Cd-rich clusters/nanoparticles with (c) d < 4 nm and (d) d > 4 nm, respectively. (For interpretation of the references to colour in this figure legend, the reader is referred to the Web version of this article.)

precipitation of dispersoids, because a higher Si content will reduce the solubility of Mn in the Al solid solution [14,27]. This can also explain the higher peak electric conductivity of the 3003SiCdCr alloy than that of other alloys. Cr is known to substitute part of Mn and Fe atoms in the α-Al(Mn,Fe)Si phase, forming α-Al(Mn,Fe,Cr)Si dispersoids [6,22]. Since Cr has a much lower diffusivity than Mn, the coarsening rate of α-Al(Mn,Fe,Cr)Si dispersoids can be much lower than that of α-Al(Mn,Fe)Si dispersoids [29]. This explains the fact that the 3003SiCdCr alloy could keep a high number density and a small size of dispersoids when heating to 500 °C. Furthermore, as the peritectic element Cr has a partitioning coefficient $k > 1$ in Al, and is different from the eutectic elements (e.g. Mn) with $k < 1$. In the as-cast alloy, the concentration of Cr in the centre of dendrite arms is higher than that at the periphery, which is opposite to the micro segregation mode of Mn. The higher concentration of Cr can compensate the depletion of Mn in the centre of dendrite arms, facilitating the nucleation and precipitation of dispersoids in the centre region of dendrite arms. This is supposed to be responsible for the more uniform distribution of dispersoids precipitated at the peak hardness temperature (Fig. 7).

4. Conclusions

In this work, significantly enhanced precipitation strengthening and thermal stability by minor additions of Cd, Cr and increased Si content in AA3003 alloy are reported. Based on the microstructural observation, effects of alloying additions on the nucleation, growth and coarsening of dispersoids in the alloys during heat treatment were systematically studied. The conclusions are drawn as follows:

1. The investigated 3003SiCdCr alloy exhibits considerably higher hardness compared to the 3003, 3003Si, 3003Cd alloys during heating between 350 and 600 °C. In the peak hardness condition, the YS of the 3003SiCdCr alloy reaches 96 ± 1 MPa, which is 39%, 19% and 12% higher than that of the 3003, 3003Si and 3003Cd alloys, respectively. The 3003SiCdCr alloy shows much higher strength than other alloys at elevated temperatures. It can keep an almost constant hardness for more than 168 h during annealing at 400 °C. After 1000 h annealing, it shows only 7.8% reduction in hardness.
2. The average diameter of dispersoids in the 3003SiCdCr alloy is smaller while the number density is much higher than that of the 3003 and 3003Cd alloys when heating at 350–550 °C. The dispersoids in the 3003SiCdCr alloy also exhibit much better coarsening resistance during high-temperature heat treatment (450–500 °C). Additionally, the distribution of dispersoids formed when heating to 450 °C is much more homogeneous across the dendrite arms in the 3003SiCdCr alloy due to the enhanced dispersoid precipitation in the centre of dendrite arms.

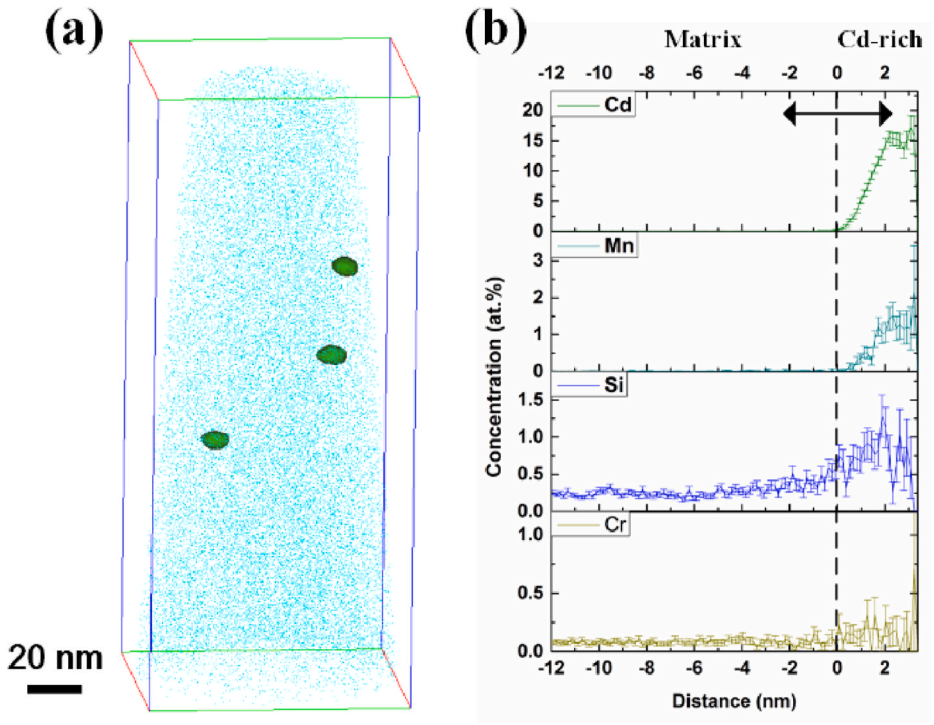

Fig. 9. (a) Cd-rich particles in the 3003SiCdCr alloy as-heated to 300 °C, the interface is defined by an isoconcentration surface at 1.5 at.% Cd; (b) proximity histogram concentration profiles showing the element distribution in/around Cd-rich particles.

3. Based on APT investigations, the nucleation process of dispersoids in the 3003SiCdCr alloy is proposed: Cd atoms first precipitate as Cd-rich atomic clusters/nanoparticles during heating at 150–200 °C; the subsequent partitioning of Mn, Si, Fe and Cr atoms into Cd-rich atomic clusters/nanoparticles leads to the local enrichment of these dispersoid-forming elements, which facilitates the heterogeneous nucleation of α-Al(Mn,Fe,Cr)Si dispersoids on Cd-rich nanoparticles at higher temperatures. This mechanism is believed to be the major reason for the refined dispersoids in the early stage of dispersoid precipitation.
4. The addition of peritectic element Cr improves the precipitation of dispersoids in the centre region of dendrite arms, forming a more uniform distribution of dispersoids during heating. Additionally, the low diffusivity of Cr in the Al(Mn,Fe,Cr)Si dispersoids is responsible for the higher number density and finer size of dispersoids at temperatures up to 500 °C, and therefore the higher thermal stability of 3003SiCdCr alloy.

Data availability statement

The raw/processed data required to reproduce these findings can be shared after time limitations.

CRediT authorship contribution statement

Feng Qian: performed material preparation and TEM characterization. **Shenbao Jin:** performed APT experiments and data reconstruction. **Di Wan:** performed SEM characterization. **Wenzhe Li:** performed mechanical tests. **Xingwang Cheng:** provided suggestions for this work. **Gang Sha:** performed APT experiments and data reconstruction. **Yanjun Li:** designed and supervised the study, All authors commented on the manuscript.

Declaration of competing interest

The authors declare that they have no known competing financial interests or personal relationships that could have appeared to influence the work reported in this paper.

Acknowledgments

This work is supported by BIT Research Fund Program for Young Scholars (Grant no. 3090012222114) and China National Key Laboratory Foundation of Science and Technology on Materials under Shock and Impact (Grant no. 6142902190402). The authors are grateful to Analysis & Testing Center at BIT, TEM Gemini Centre at NTNU (NORTEM infrastructure, Grant 197405) and Materials Microstructural Characterization Centre at NJUST.

References

[1] E. Clouet, L. Laé, T. Epicier, W. Lefebvre, M. Nastar, A. Deschamps, Complex precipitation pathways in multicomponent alloys, Nat. Mater. 5 (2006) 482–488, https://doi.org/10.1038/nmat1652.
[2] A. Tolley, V. Radmilovic, U. Dahmen, Segregation in Al3(Sc,Zr) precipitates in Al–Sc–Zr alloys, Scripta Mater. 52 (2005) 621–625, https://doi.org/10.1016/j.scriptamat.2004.11.021.
[3] K.E. Knipling, D.N. Seidman, D.C. Dunand, Ambient- and high-temperature mechanical properties of isochronally aged Al–0.06Sc, Al–0.06Zr and Al–0.06Sc–0.06Zr (at.%) alloys, Acta Mater. 59 (2011) 943–954, https://doi.org/10.1016/j.actamat.2010.10.017.
[4] C. Booth-Morrison, D.C. Dunand, D.N. Seidman, Coarsening resistance at 400°C of precipitation-strengthened Al–Zr–Sc–Er alloys, Acta Mater. 59 (2011) 7029–7042, https://doi.org/10.1016/j.actamat.2011.07.057.
[5] H. Hirasawa, Precipitation process of Al-Mn and Al-Cr supersaturated solid solution in presence of age hardening phases, Scripta Metall. 9 (1975) 955–958, https://doi.org/10.1016/0036-9748(75)90551-7.
[6] L. Lodgaard, N. Ryum, Precipitation of dispersoids containing Mn and/or Cr in Al–Mg–Si alloys, Mater. Sci. Eng. 283 (2000) 144–152, https://doi.org/10.1016/S0921-5093(00)00734-6.
[7] Y.J. Li, L. Arnberg, Quantitative study on the precipitation behavior of dispersoids in DC-cast AA3003 alloy during heating and homogenization, Acta Mater. 51 (2003) 3415–3428, https://doi.org/10.1016/S1359-6454(03)00160-5.
[8] E. Nes, The effect of a fine particle dispersion on heterogeneous recrystallization, Acta Metall. 24 (1976) 391–398, https://doi.org/10.1016/0001-6160(76)90059-6.
[9] Y. Kwag, J.G. Morris, The effect of structure on the mechanical behavior and stretch formability of constitutionally dynamic 3000 series aluminum alloys, Mater. Sci. Eng. 77 (1986) 59–74, https://doi.org/10.1016/0025-5416(86)90354-X.

[10] Y.J. Li, A.M.F. Muggerud, A. Olsen, T. Furu, Precipitation of partially coherent α-Al (Mn,Fe)Si dispersoids and their strengthening effect in AA 3003 alloy, Acta Mater. 60 (2012) 1004–1014, https://doi.org/10.1016/j.actamat.2011.11.003.
[11] K. Liu, X.-G. Chen, Development of Al–Mn–Mg 3004 alloy for applications at elevated temperature via dispersoid strengthening, Mater. Des. 84 (2015) 340–350, https://doi.org/10.1016/j.matdes.2015.06.140.
[12] K. Liu, X.-G. Chen, Influence of heat treatment and its sequence on elevated-temperature properties of Al-Mn-Mg 3004 alloy, Mater. Sci. Eng. 697 (2017) 141–148, https://doi.org/10.1016/j.msea.2017.05.027.
[13] A.R. Farkoosh, D.C. Dunand, D.N. Seidman, Solute-induced strengthening during creep of an aged-hardened Al-Mn-Zr alloy, Acta Mater. (2021) 117268, https://doi.org/10.1016/j.actamat.2021.117268.
[14] A.M.F. Muggerud, E.A. Mørtsell, Y. Li, R. Holmestad, Dispersoid strengthening in AA3xxx alloys with varying Mn and Si content during annealing at low temperatures, Mater. Sci. Eng. 567 (2013) 21–28, https://doi.org/10.1016/j.msea.2013.01.004.
[15] K. Liu, X.-G. Chen, Evolution of intermetallics, dispersoids, and elevated temperature properties at various Fe contents in Al-Mn-Mg 3004 alloys, Metall. Mater. Trans. B 47 (2016) 3291–3300, https://doi.org/10.1007/s11663-015-0564-y.
[16] Z. Li, Z. Zhang, X.-G. Chen, Microstructure, elevated-temperature mechanical properties and creep resistance of dispersoid-strengthened Al-Mn-Mg 3xxx alloys with varying Mg and Si contents, Mater. Sci. Eng. 708 (2017) 383–394, https://doi.org/10.1016/j.msea.2017.10.013.
[17] Z. Li, Z. Zhang, X.-G. Chen, The influence of Cu addition on dispersoid formation and mechanical properties of Al-Mn-Mg 3004 alloy, Metals 8 (2018), https://doi.org/10.3390/met8030155.
[18] Z. Li, Z. Zhang, X.-G. Chen, Improvement in the mechanical properties and creep resistance of Al-Mn-Mg 3004 alloy with Sc and Zr addition, Mater. Sci. Eng. 729 (2018) 196–207, https://doi.org/10.1016/j.msea.2018.05.055.
[19] K. Liu, H. Ma, X.-G. Chen, Enhanced elevated-temperature properties via Mo addition in Al-Mn-Mg 3004 alloy, J. Alloys Compd. 694 (2017) 354–365, https://doi.org/10.1016/j.jallcom.2016.10.005.
[20] F. Qian, S. Jin, G. Sha, Y. Li, Enhanced dispersoid precipitation and dispersion strengthening in an Al alloy by microalloying with Cd, Acta Mater. 157 (2018) 114–125, https://doi.org/10.1016/j.actamat.2018.07.001.
[21] A.R. Farkoosh, X. Grant Chen, M. Pekguleryuz, Dispersoid strengthening of a high temperature Al–Si–Cu–Mg alloy via Mo addition, Mater. Sci. Eng. 620 (2015) 181–189, https://doi.org/10.1016/j.msea.2014.10.004.
[22] L. Lodgaard, N. Ryum, Precipitation of chromium containing dispersoids in Al–Mg–Si alloys, Mater. Sci. Technol. 16 (2000) 599–604, https://doi.org/10.1179/026708300101508315.
[23] C. Flament, J. Ribis, J. Garnier, T. Vandenberghe, J. Henry, A. Deschamps, Electron irradiation-enhanced core/shell organization of Al(Cr, Fe, Mn)Si dispersoids in Al–Mg–Si alloys, Philos. Mag. A 95 (2015) 906–917, https://doi.org/10.1080/14786435.2015.1009959.
[24] D. Simonovic, M.H.F. Sluiter, Impurity diffusion activation energies in Al from first principles, Phys. Rev. B 79 (2009), 054304, https://doi.org/10.1103/PhysRevB.79.054304.
[25] Y. Du, Y. Chang, B. Huang, W. Gong, Z. Jin, H. Xu, Z. Yuan, Y. Liu, Y. He, F.-Y. Xie, Diffusion coefficients of some solutes in fcc and liquid Al: critical evaluation and correlation, Mater. Sci. Eng. 363 (2003) 140–151, https://doi.org/10.1016/S0921-5093(03)00624-5.
[26] F. Qian, D. Zhao, E.A. Mørtsell, S. Jin, J. Wang, C.D. Marioara, S.J. Andersen, G. Sha, Y. Li, Enhanced nucleation and precipitation hardening in Al-Mg-Si(-Cu) alloys with minor Cd additions, Mater. Sci. Eng. 792 (2020) 139698.
[27] Y. Li, L. Arnberg, Precipitation of dispersoids in DC-cast AA3103 alloy during heat treatment BT - essential readings in light metals: volume 3 cast shop for aluminum production, in: J.F. Grandfield, D.G. Eskin (Eds.), Essent. Readings Light Met., Springer International Publishing, Cham, 2016, pp. 1021–1027, https://doi.org/10.1007/978-3-319-48228-6_129.
[28] B.D. Saller, G. Sha, L.M. Yang, F. Liu, S.P. Ringer, J.M. Schoenung, Iron in solution with aluminum matrix after non-equilibrium processing: an atom probe tomography study, Phil. Mag. Lett. 97 (2017) 118–124, https://doi.org/10.1080/09500839.2017.1292055.
[29] Q. Du, Y.J. Li, Effect modeling of Cr and Zn on microstructure evolution during homogenization heat treatment of AA3xxx alloys, Trans. Nonferrous Met. Soc. China 24 (2014) 2145–2149, https://doi.org/10.1016/S1003-6326(14)63325-2.